



# LUND UNIVERSITY

## **A comparison between direct numerical simulation and experiment of the turbulent burning velocity-related statistics in a turbulent methane-air premixed jet flame at high Karlovitz number**

Wang, Haiou; Hawkes, Evatt R.; Zhou, Bo; Chen, Jacqueline H.; Li, Zhongshan; Aldén, Marcus

*Published in:*  
Proceedings of the Combustion Institute

*DOI:*  
[10.1016/j.proci.2016.07.104](https://doi.org/10.1016/j.proci.2016.07.104)

2017

[Link to publication](#)

### *Citation for published version (APA):*

Wang, H., Hawkes, E. R., Zhou, B., Chen, J. H., Li, Z., & Aldén, M. (2017). A comparison between direct numerical simulation and experiment of the turbulent burning velocity-related statistics in a turbulent methane-air premixed jet flame at high Karlovitz number. *Proceedings of the Combustion Institute*, 36(2), 2045–2053. <https://doi.org/10.1016/j.proci.2016.07.104>

*Total number of authors:*  
6

*Creative Commons License:*  
CC BY

### **General rights**

Unless other specific re-use rights are stated the following general rights apply:  
Copyright and moral rights for the publications made accessible in the public portal are retained by the authors and/or other copyright owners and it is a condition of accessing publications that users recognise and abide by the legal requirements associated with these rights.

- Users may download and print one copy of any publication from the public portal for the purpose of private study or research.
- You may not further distribute the material or use it for any profit-making activity or commercial gain
- You may freely distribute the URL identifying the publication in the public portal

Read more about Creative commons licenses: <https://creativecommons.org/licenses/>

### **Take down policy**

If you believe that this document breaches copyright please contact us providing details, and we will remove access to the work immediately and investigate your claim.

LUND UNIVERSITY

PO Box 117  
221 00 Lund  
+46 46-222 00 00

**Title page:**

**A Comparison between Direct Numerical Simulation and Experiment of the  
Turbulent Burning Velocity-Related Statistics in a Turbulent Methane-Air  
Premixed Jet Flame at High Karlovitz Number**

Haiou Wang<sup>a,\*</sup>, Evatt R. Hawkes<sup>a,b</sup>, Bo Zhou<sup>c</sup>, Jaqueline H. Chen<sup>d</sup>, Zhongshan Li<sup>c</sup>, Marcus Aldén<sup>c</sup>

<sup>a</sup>*School of Mechanical and Manufacturing Engineering, The University of New South Wales, NSW 2052 Australia*

<sup>b</sup>*School of Photovoltaic and Renewable Energy Engineering, The University of New South Wales, NSW 2052*

*Australia*

<sup>c</sup>*Division of Combustion Physics, Lund University, P.O. Box 118, S221 00 Lund, Sweden*

<sup>d</sup>*Sandia National Laboratories, Livermore, CA 94550, USA*

\*Corresponding author: [haiou.wang@unsw.edu.au](mailto:haiou.wang@unsw.edu.au)

This is the peer reviewed version of the following article: [H. Wang, E. R. Hawkes, B. Zhou, J. H. Chen, Z.S. Li, M. Aldén, 'A Comparison between Direct Numerical Simulation and Experiment of the Turbulent Burning Velocity-Related Statistics in a Turbulent Methane-Air Premixed Jet Flame at High Karlovitz Number', **Proc. Combust. Inst.** **36**, 2045-2053 (2017).], which has been published in final form at <https://doi.org/10.1016/j.proci.2016.07.104>

# **Comparison between Direct Numerical Simulation and Experiment of the Turbulent Burning Velocity-Related Statistics in a Turbulent Methane-Air Premixed Jet Flame at High Karlovitz Number**

Haiou Wang<sup>a,\*</sup>, Evatt R. Hawkes<sup>a,b</sup>, Bo Zhou<sup>c</sup>, Jaqueline H. Chen<sup>d</sup>, Zhongshan Li<sup>c</sup>, Marcus Aldén<sup>c</sup>

<sup>a</sup>*School of Mechanical and Manufacturing Engineering, The University of New South Wales, NSW 2052 Australia*

<sup>b</sup>*School of Photovoltaic and Renewable Energy Engineering, The University of New South Wales, NSW 2052*

*Australia*

<sup>c</sup>*Division of Combustion Physics, Lund University, P.O. Box 118, S221 00 Lund, Sweden*

<sup>d</sup>*Sandia National Laboratories, Livermore, CA 94550, USA*

\*Corresponding author: haiou.wang@unsw.edu.au

*Submitted to:* 36<sup>th</sup> International Symposium on Combustion

*Colloquium:* Turbulent Flames.

*Total length:* 5788 words equivalent using Method 1.

*Main text:* 4102

*Equations:* 30

*References:* 664

*Figures:* 992, as follows: Fig. 1, 151; Fig. 2, 180; Fig. 3, 131; Fig. 4, 149; Fig. 5, 241; Fig. 6, 140.

Affirmation to pay color reproduction charges if applicable: applicable

**Abstract:** Three-dimensional (3D) direct numerical simulation (DNS) of an experimental turbulent premixed jet flame at high Karlovitz number was carried out. The DNS resolution adequately resolves both the flame and turbulence structures. A reduced chemical mechanism for premixed CH<sub>4</sub>/air flames with NO<sub>x</sub> based on GRI-Mech3.0 was used, including 268 elementary reactions, and 28 transported species. The same post-processing methods were applied to both the DNS and experimental data to evaluate the turbulent burning velocity-related quantities, namely flame surface density (FSD), and flame curvature. Fairly good agreement was achieved for the 2D comparisons. The DNS data were further analysed and provide 3D statistics unattainable from the experiment. The ratio of the 2D and 3D flame surface densities was estimated. The results are comparable with other values reported for various experimental flames. The 2D and 3D flame curvatures were also compared and their distributions are shown to be quite different owing to the round on-average geometry of the flame as well as the formation of cusps on the instantaneous flame front. Instantaneous images of the heat release surrogate [CH<sub>2</sub>O][OH] between the experiment and DNS agreed qualitatively. It is confirmed using the DNS that [CH<sub>2</sub>O][OH] correlates with heat release rate well even at high turbulent intensities. The inner structures of the flame were compared between the DNS and experiment in terms of the joint PDFs of OH concentration and temperature. Generally good agreement was obtained; discrepancies may be due to the inconsistency of assumed equilibrium levels of certain species in the co-flow.

**Keywords:** Direct numerical simulation, high Karlovitz number, lean premixed combustion, turbulent burning rate

## 1. Introduction

Combined cycle gas turbines are expected to play an increasing role in energy systems. In addition to being the most efficient and lowest CO<sub>2</sub> emitting combustion-based energy technology that is widely available, they have a fast starting capability that can complement high penetration renewable energy. To reduce NO<sub>x</sub> emissions, many modern gas turbines run in a lean premixed mode. However, lean premixed combustion is susceptible to operability issues including combustion instability, blowout and flashback [1]. To enable improved designs, a better understanding of premixed turbulent combustion is required. In particular, one fundamental issue that underpins all these problems is the interaction of intense turbulence with relatively weak flames, due to high dilution with air.

In turbulent premixed combustion, a non-dimensional parameter, the Karlovitz number (Ka), has been introduced to classify scenarios of turbulence/flame interactions [2]. Ka is defined as the ratio of the flame and Kolmogorov time scales:  $Ka = \tau_L / \tau_\eta$ . For  $Ka < 1$ , turbulence does not enter the preheat or reaction zone, and structures that are locally similar to laminar flames are observed. However, in lean premixed gas turbines, flames are located in the thin ( $100 > Ka > 1$ ) or broken ( $Ka > 100$ ) reaction zones regime, where Kolmogorov scales can penetrate and disrupt the flame structure. In these regimes, the inner structure of the flame is not the same as a laminar flame, as there may be broadening of the preheat and/or reaction zones, and local extinction.

Relative to the situation at low Ka, understanding of flames in high Ka regimes is not particularly advanced. This has motivated a number of experimental and direct numerical simulation (DNS) studies of high Ka premixed combustion. The DNS studies are first reviewed. Early work focused on flame-vortex interactions to understand and stretching and quenching effects [3]. Later studies focused on isotropic turbulence, including two-dimensional (2D) detailed chemistry DNS [4-6], three-dimensional (3D) one-step chemistry DNS [7], and 3D detailed chemistry DNS [8-11]. More recently, moderate Ka cases have been reported having mean shear and non-trivial geometry, including spatially developing slot jet methane-air flames [12, 13] and temporally evolving, slot jet hydrogen flames [14, 15]. Another notable trend in the literature is that DNS of real laboratory flames has recently become possible. Work in this direction included DNS of a rod-stabilised premixed flame [16], a slot Bunsen flame [17], and a swirl-stabilised flame [18]. However, all of these computations are at a relatively low Ka.

There has also been significant interest in achieving high Ka conditions in the laboratory, which have reported features such as distributed preheat and/or reaction zones, and local extinctions [19, 20]. Because of the large burner size and high Reynolds number (Re) of these experiments, DNS is currently not feasible; however recently a more approachable experiment having a smaller 1.5 mm burner and some moderate Re conditions was reported by Lund University [21]. This study reported a series of co-flowing turbulent premixed jet flame experiments at high Ka conditions in the thin and broken reaction zones regimes. The Re ranged from 6,000 to 40,000 and Ka varied from 25 to 1470. Simultaneous planar laser-induced fluorescence (PLIF) measurements of OH and CH<sub>2</sub>O and Rayleigh scattering measurements of temperature were carried out. Among the experimental conditions, of particular interest and feasibility for performing DNS is a methane-air premixed flame at high Ka and moderate Re (10,510) and at an equivalence ratio of 0.7. This flame is selected as the target flame for the present DNS study.

The particular objectives of this study are to examine key statistics in the DNS and experiment, including the flame surface density (FSD)  $\Sigma$ , flame curvatures, and experimental surrogates for heat release rate. The selection of these quantities is motivated by their availability in the experiments and their relevance to the turbulent burning velocity,  $S_T$ , which is outlined in the following. FSD influences  $S_T$  explicitly through the expression  $S_T = S_L \cdot I_\theta \int \Sigma d\eta$  [22], where  $S_L$  is the laminar flame velocity,  $I_\theta$  is the stretch factor, and  $\eta$  is the mean flame propagation direction. The turbulent burning velocity is also affected by stretch, induced both by tangential strain rate and curvature stretch, both directly in the production/destruction of  $\Sigma$  and indirectly via effects on  $I_\theta$ . Hence, flame curvature plays an important role in determining the overall burning rate. Finally, arguably the most direct measure of burning velocity would be determined by local heat release rates; however, direct measurement of local heat release rate is not possible. It was previously shown in laminar flame-vortex interaction simulations, the product imaging of OH and CH<sub>2</sub>O is a good surrogate of heat release rate [23, 24], as it is a direct measurement of the reaction rate  $\text{CH}_2\text{O} + \text{OH} = \text{H}_2\text{O} + \text{HCO}$ , and provides an estimate of the production rate of HCO. However, the adequacy of this heat release surrogate has not been verified for high Ka flames.

The present study aims to perform direct comparisons of the above-mentioned statistics associated with turbulent burning velocity obtained from DNS and experiment. To the best of the authors' knowledge, this is the first such direct comparison for a laboratory-scale

flame at high Ka. Beyond cross-validation of the DNS and the experiment for 2D statistics related to FSD and curvature, the DNS further establishes differences between 2D and 3D FSD and curvature statistics.

The paper is organised as follows. Section 2 describes the computational approach and key parameters. Section 3 describes the data processing method used to extract FSD and curvature statistics. Statistical comparisons between model and experiment, an evaluation of 2D/3D differences using the DNS, and an evaluation the adequacy of a surrogate heat release measurement and discussion are presented in Section 4 before drawing conclusions in Section 5.

## 2. Numerical Methods

The experimental configuration is a round, piloted turbulent premixed methane-air burner operating at atmospheric pressure [21]. The jet bulk velocity is  $U_b=110$  m/s, the jet equivalence ratio is  $\phi=0.7$ , and the jet temperature is  $T_j=300$  K. The jet diameter is  $D=1.5$  mm and the jet Re based on  $U_b$  and  $D$  is  $Re=10,510$ . The small diameter and moderate Re render the DNS computationally feasible, while retaining interesting features of high Ka. A wide laminar  $CH_4$ /air co-flowing pilot flame having co-flow velocity  $U_c$  of 1.8 m/s, measured temperature  $T_c$  of 1800K and equivalence ratio  $\phi$  of 0.9 is used to stabilise the jet flame. At these conditions, the laminar flame velocity  $S_L$  is 0.19 m/s, the flame thermal thickness  $\delta_L$  is 0.66 mm, and the flame time scale  $\tau_L=\delta_L/S_L$  is 3.4 ms. A photograph of the flame's natural luminosity is shown in Fig. 1a.

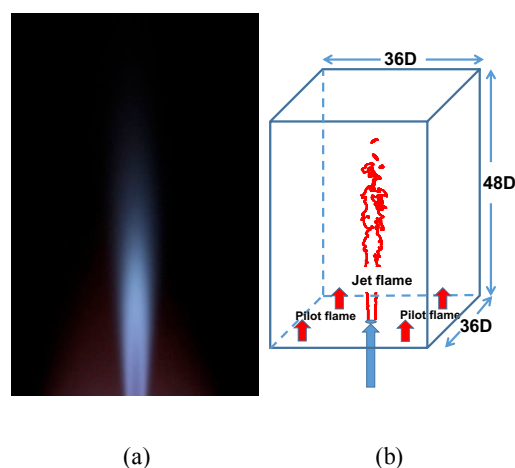


Figure 1. (a) Photograph of the turbulent flame from the experiment. (b) Schematic of the computational domain for DNS.

The DNS models the configuration of a premixed-fuel air jet issuing into an effectively infinite pilot flame. This is reasonable

because the pilot is  $40D$  wide, which is large enough to completely shield the flame from ambient air. Fig. 1b illustrates the DNS configuration, where the instantaneous flame front is, denoted by the progress variable iso-surface (defined in Section 3), delineated in red. The mean jet axial velocity profile at the inlet is specified to match that of the experiment using a power law velocity profile for an axisymmetric fully developed turbulent flow [25]. Superimposed on this mean profile is a turbulence field with a fluctuation velocity of 4% of the bulk velocity, obtained by generating an auxiliary homogeneous isotropic turbulence field based on a prescribed energy spectrum [26].  $Ka$  at the inlet is 253. The Damköhler number ( $Da$ ) defined as the ratio of the integral time scale  $\tau_I$  to the flame time scale  $\tau_L$  is 0.054. For the large  $Ka$  and small  $Da$  in the present study, all turbulence time scales are smaller than the flame time scale, and the flame is in the broken reaction zones regime [2].

In the experiment the flame is attached to the burner, and the temperature and species profiles are somewhat uncertain near the burner due to a number of factors including heat loss to the burner, flame stretch effects, and possible chemical reactions on the burner surface. Therefore, we specify the following simple profile for a scalar  $\psi$ :

$$\psi = \psi_c + \frac{\psi_j - \psi_c}{2} \left( 1 + \frac{\tanh(D/2 - r)}{\delta} \right) \quad (1)$$

where  $\psi_j$  and  $\psi_c$  respectively denote the values of  $\psi$  in the jet and co-flow,  $r$  is the radial distance and  $\delta$  is the thickness of the transition.  $\psi_c$  is determined from an equilibrium calculation of a  $CH_4$ /air mixture with  $\phi=0.9$  at a defined temperature of 1800 K.  $\psi_j$  is computed based on a  $CH_4$ /air mixture with  $\phi=0.7$  at 300 K. For  $r < D/2$ ,  $\delta$  is specified as  $0.08D$ ; for  $r > D/2$ ,  $\delta$  is the half width of the burner surface, i.e. 3.5 mm to mimic the smooth transition between the co-flow and main jet. This simple approach undoubtedly introduces some errors in the near burner region, but the main focus of this study is on the downstream region, which should be determined mainly by the jet and pilot conditions.

The physical domain is large owing to the long flame length:  $L_x \times L_y \times L_z = 48D \times 36D \times 36D$  in the streamwise  $x$  and lateral directions  $y$  and  $z$ , respectively, as illustrated in Fig. 1b. The resolution is chosen to adequately resolve both the flame and turbulence. A uniform grid spacing of  $\Delta x = 30 \mu m$  is used in the streamwise direction  $x$ , while algebraic stretching is used in the lateral directions  $y$  and  $z$  outside of the shear zone. The grid in the  $y$  ( $z$ ) direction is uniform with  $\Delta y$  ( $\Delta z$ ) =  $30 \mu m$  in the region between  $y/D$  ( $z/D$ ) = -5 and 5, and gradually

stretched outside of this region with a maximum relative stretching rate of 1.9%. Approximately 22 grid points across  $\delta_L$  are obtained with this spatial resolution. In the present high Ka case, the resolution of turbulence is more demanding. The Kolmogorov scale, defined as  $\eta = (\nu^3 / \varepsilon)^{1/4}$ , has a minimum of 10  $\mu\text{m}$  in a narrow region near the potential core, where the flame does not overlap. The usual criterion for turbulence resolution  $\eta / \Delta x > 0.5$  [27] is satisfied elsewhere. Thus, the smallest scales of the turbulent flow are reasonably resolved in the flame region. The resultant grid is  $N_x \times N_y \times N_z = 2400 \times 900 \times 900$ . To flush out initialisation artefacts, the simulation was first advanced for  $10\tau_j$  on a half-resolved grid, where  $\tau_j$  is the flow through time defined as  $\tau_j = L_x / U_b$ . The results were then mapped to the fine grid. The solution was advanced for another  $10\tau_j$  to provide stationary statistics. It was found that statistical results of the half-resolution run and the production run are very similar, confirming the resolution is adequate.

The DNS code ‘S3D’ was employed to solve the compressible transport equations for continuity, momenta, species mass fractions and total energy [28]. The code uses a fourth-order Runge-Kutta method [29, 30] and a skew-symmetric, eighth-order explicit finite difference spatial scheme. A tenth-order filter was applied to damp high-wave number oscillations. A previously published reduced chemical mechanism for premixed  $\text{CH}_4/\text{air}$  flames with  $\text{NO}_x$  chemistry derived from GRI-Mech 3.0 was employed [31]. The mechanism contains 268 elementary reactions and 44 species, of which 16 species are identified as quasi-steady state species. The remaining 28 species are transported on the DNS grid. The mechanism has been validated against the detailed mechanism comprehensively [31]. The species Lewis numbers are assumed to be constant.

The simulation was performed on a Cray XC-40 located at the Pawsey Supercomputing Centre in Australia and required 10 million CPU-hours on 19,200 Intel Xeon Haswell processor cores for approximately 22 days.

### 3. Data Processing Methodology

In this section, methods for constructing the FSD and flame curvature statistics from the experiment and computation are described. Two different methods are utilised to extract the flame front. In many previous DNS studies [12-15], flame fronts are typically defined using the mass fraction of a major species. Major species are, however, not available in the experiment, and the temperature is not an optimal flame front marker due its limited signal-to-noise ratio. Therefore, flame fronts are extracted from OH images, being referred as

the first method for the flame front determination. A  $2 \times 2$  pixel filter was applied to reduce noise. The OH intensity is first normalised by its maximum value. As the flame is weaker upstream (see Fig. 1a), the normalisation is performed locally in each row (corresponding to a given axial location) of the image. Two iso-lines of the image are identified using a threshold level of 0.25. One is in the fuel consumption layer, corresponding to the location of the maximum heat release rate. The other one is in the oxidation layer, which is not desirable. As  $\text{CH}_2\text{O}$  concentration in the oxidation layer is negligible, the second iso-line is excluded by multiplying the OH image with a binarised  $\text{CH}_2\text{O}$  concentration image. The remaining iso-line defines the flame front and the spatial coordinates of the points along the flame front are recorded.

. Since OH concentration is smaller upstream due to a weaker flame, OH cannot be used to extract the 3D flame front unambiguously. Local normalization of OH concentration would result in discontinuity of the iso-surface, while this discontinuity is insignificant in the 2D case. Therefore, a second method is to extract the 3D flame front from the DNS. The iso-surface  $c=0.8$  is chosen to denote the flame front, where  $c$  is the progress variable defined based on the  $\text{O}_2$  mass fraction [12, 13], corresponding to the location of maximum heat release rate in the unstrained laminar flame.

To calculate FSD, the instantaneous flame front is binned into an interrogation box of size  $0.375 \times 0.375 \text{ mm}^2$ . The FSD values are insensitive to the size of the interrogation box. The flame length in each box  $L$  is computed based on the spatial coordinates of the discretised points, and subsequently divided by the area of the interrogation box,  $A$ . This procedure is repeated for each image. The results are then averaged to obtain the spatial distribution of FSD, i.e.  $\Sigma_2 = (\sum_{i=1}^{N_s} L_i) / (N_s A)$ , where  $N_s$  is the number of images. In the DNS, a 2D OH concentration image of a typical  $x$ - $r$  plane is exported for each snapshot; for consistency, the filtering from the experiment [21] was also applied to the DNS OH images. The same procedure described above is used to compute FSD from the DNS.

As most of experimental measurements were performed in two spatial dimensions as it is in the present study, it is necessary to develop a theoretical correction of the 2D measurements to estimate the corresponding 3D quantities [33, 34]. Therefore, a comparison of the 2D and 3D FSD evaluated from the DNS is performed using the  $\text{O}_2$ -based flame front definition. The 3D FSD  $\Sigma_3$  is calculated as the flame surface area per unit volume.

Due to preferential diffusion effects, the local burning rate correlates strongly with curvature even at large turbulence intensities [5]. In the present study, flame curvature statistics are extracted from both the experiment and DNS in 2D first, and then DNS is used to compare 2D and 3D statistics. To calculate the 2D flame curvature, the instantaneous flame front extracted from the OH images using the first method is employed. The flame curvature at each discretised point along the flame front is then determined [18]. The flame curvature is positive (negative) when the flame front is convex (concave) towards the reactant.

To calculate the 3D curvature from the DNS, the  $O_2$ -based flame front definition is used. The 3D curvature is calculated as  $\nabla \cdot \mathbf{n}$ , where  $\mathbf{n}$  is the flame normal defined as  $\mathbf{n} = -\nabla c / |\nabla c|$ . Similarly, a 2D curvature is evaluated as  $\nabla_2 \cdot \mathbf{n}_2$ , where  $\mathbf{n}_2 = -\nabla_2 c / |\nabla_2 c|$  and  $\nabla_2$  denotes the vector-differential operator in  $x-r$  space.

## 4. Results and Discussions

### 4.1 Comparison of Flame Surface Density

Figure 2 shows a comparison of the FSD contours from the DNS and experiment. The same data-processing has been applied to both the DNS and experiment, enabling a direct comparison. The flame has two statistically symmetric branches in the  $x-r$  plane. In the upstream region, the FSD values are high and the distribution is narrow. As the flame develops, the FSD progressively becomes lower in magnitude and wider in spatial extent. Finally, the two branches merge due to complete consumption of the reactants and the corresponding flame annihilation. Overall there is good agreement in the FSD between the DNS and experiment, both in terms of their spatial evolution and their magnitude. The DNS profile appears slightly wider, which could be attributed to a few factors; for example, the coflow product compositions could be different from equilibrium as it was assumed in the DNS. More quantitatively, the comparisons of the integral of the 2D FSD over the radial direction [35] between the DNS and experiment are displayed in Fig. 2c, and very good agreement is obtained. The flame surface area approaches its maximum around  $x/D=24$  and the flame length is approximately  $38D$  as shown from both profiles.

The profiles of FSD at two representative locations  $x/D=10$  and  $24$  are shown in Figs. 3a and 3b, respectively. The left half of the figure shows the FSD results computed from the first method, while the right shows those computed from the second. It is seen that the

FSD of the DNS and experiment quantitatively agree with only a minor discrepancy in the position of the flame at  $x/D=10$  and the position and width at  $x/D=24$ . The simulated flame appears to be slightly shifted radially outwards compared to the experimental flame, consistent with the observation in Figs. 2a and 2b.

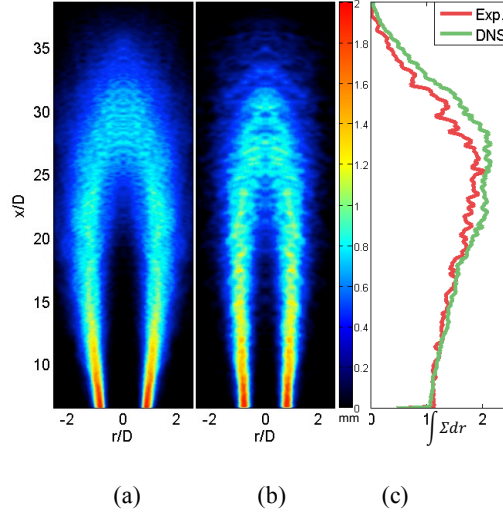


Figure 2. Comparison of the flame surface density  $\Sigma$  distribution: (a) DNS and (b) experiment. (c) Comparison of the integral of flame surface density in the radial direction  $\int \Sigma(x, r) dr$ .

Figure 3 also shows that  $\Sigma_2$  calculated with the second  $O_2$ -based method is slightly larger than that computed with the first OH-based method at  $x/D=10$ , while they are comparable further downstream at  $x/D=24$ . This may be due to the greater degree of small-scale wrinkles at  $x/D=10$ , which might be smoothed by filtering the images in the first method but not in the second method. At  $x/D=24$ , the wrinkling scales are larger, and the effects of filtering on the FSD calculation are minimised. As a result, there is a very good agreement between the two methods of calculating FSD.

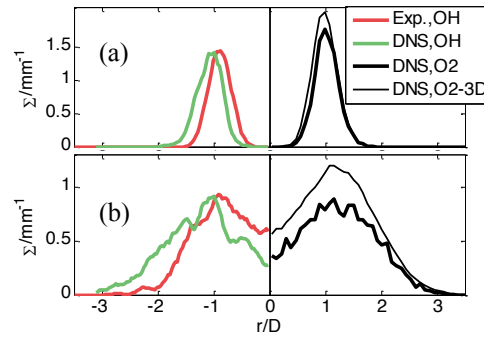


Figure 3. Comparison of  $\Sigma$  along the radial direction at (a)  $x/D=10$  and (b)  $x/D=24$ .

Because the experimental measurements are 2D, the FSD is underestimated. The extent of this underestimation can be assessed

using the DNS. If we assume that the angle  $\varphi$  between the flame normal and the measurement plane has an isotropic distribution, it is readily shown that  $\Sigma_3/\Sigma_2 = 4/\pi \approx 1.27$  [33, 34]. Close to the nozzle,  $\Sigma_3/\Sigma_2$  is expected to be unity because the flame is unwrinkled and  $\varphi$  is zero. Figs 3a and 3b show the profiles of  $\Sigma_3$  and  $\Sigma_2$  at  $x/D=10$  and 24, respectively. It is observed that  $\Sigma_3$  is generally larger than  $\Sigma_2$ . The ratio  $\Sigma_3/\Sigma_2$  at the location of peak FSD is 1.14 and 1.35 at  $x/D=10$  and 24, respectively. Comparable values have been reported for various experimental flames [35, 36]. The results indicate that the flame is more wrinkled at  $x/D = 24$  than at  $x/D = 10$ , and the distribution of the angle  $\varphi$  is different from isotropic. A detailed analysis of the flame orientations is not within the present scope, but will be explored in the future.

#### 4.2 Comparison of Flame Curvature

Figure 4 shows the PDFs of the flame curvature at  $x/D=10$  and 24. The DNS results evaluated using the first OH-based method are almost identical to the experimental results. Only a slight discrepancy is found at small curvature. This indicates that the DNS and experiment have very similar wrinkling scales, consistent with the discussion of Fig. 2c. The PDFs of the 2D curvature using the second O<sub>2</sub>-based method exhibit similar shapes. However, they are slightly shifted towards positive curvature. This indicates slightly different wrinkling scales for the OH and O<sub>2</sub> fields; some differences should be expected due to their differing reactivity and diffusivities.

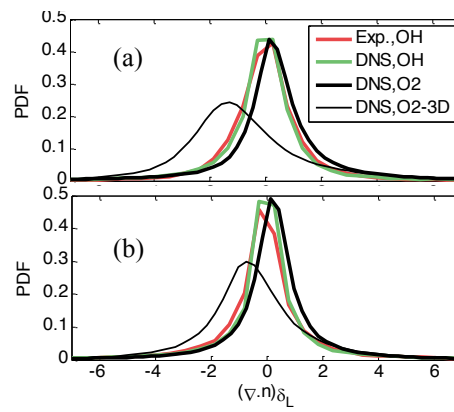


Figure 4. Comparison of flame curvature PDFs at (a)  $x/D=10$  and (b)  $x/D=24$ .

The 2D curvature PDFs are symmetric and their means are near zero. However, care should be taken when interpreting the 2D curvature results. The 3D curvature PDFs shown in Fig. 4 reveal that the curvature distribution is positively skewed and the mean is negative. For a round jet flame, the mean flame front is nearly cylindrical and convex towards the product. As a result, the flame curvature

has a negative, non-zero mean. The curvature of the mean flame front could be roughly estimated as  $-1/R(x)$ , where  $R(x)$  is the distance of the mean flame front to the centerline at the axial location  $x$ . The DNS results show that  $R$  increases with  $x$  until  $x/D=24$ , where it peaks. This explains why the mean curvature at  $x/D=24$  (Fig. 4b) is smaller than that at  $x/D=10$  (Fig. 4a).

### 4.3 Comparison of Flame Structure

The most direct measure of the turbulent burning rate would be a local evaluation of the heat release rate, however its direct measurement is not possible. Paul and Najm [23] reported that the product of  $\text{CH}_2\text{O}$  and  $\text{OH}$  concentrations is a good surrogate of the heat release rate in laminar flame-vortex interactions, but there have been no such comparisons for high  $Ka$  flames. PLIF imaging of  $[\text{CH}_2\text{O}]$  and  $[\text{OH}]$  facilitates the utilisation of this approach. Figs. 5a and 5b shows a comparison of the instantaneous images of  $[\text{CH}_2\text{O}][\text{OH}]$  between the experiment and DNS. There is qualitative agreement between the images, indicating similar turbulence/chemistry interactions. The validity of  $[\text{CH}_2\text{O}][\text{OH}]$  as a heat release rate surrogate is examined using the DNS results. Fig. 5c shows the heat release rate field in the same scenario. It is seen that the distributions of  $[\text{CH}_2\text{O}][\text{OH}]$  and heat release rate are very similar even for this high  $Ka$  flame. The good correlations between  $[\text{CH}_2\text{O}][\text{OH}]$  and heat release rate are further confirmed by the scatter plots (Fig. 5d). Downstream, some weak heat release rate is observed on the product side where  $[\text{CH}_2\text{O}][\text{OH}]$  is negligible. This is due to the oxidation reactions of  $\text{CO}$  and  $\text{H}_2$ , i.e.  $\text{CO}+\text{OH}=\text{CO}_2+\text{H}$  and  $\text{H}_2+\text{OH}=\text{H}_2\text{O}+\text{H}$ , occurring downstream where  $\text{CO}$ ,  $\text{H}_2$  and  $\text{OH}$  are relatively abundant. The present good agreement between  $[\text{CH}_2\text{O}][\text{OH}]$  and heat release rate could in principle be used to evaluate  $I_0$ , i.e.,  $I_0 = \int ([\text{CH}_2\text{O}][\text{OH}]) / ([\text{CH}_2\text{O}]_l [\text{OH}]_l) d\mathbf{n}$ , where the subscript  $l$  denotes the laminar quantities.

Finally, the inner flame structure is compared between the DNS and experiment in terms of the joint PDFs of  $\text{OH}$  concentration temperature at  $x/D = 10$  and  $24$  as shown in Fig. 6. It is seen that at  $x/D = 24$ , the joint PDFs are in good agreement. At  $x/D=10$ ,  $\text{OH}$  concentration from the DNS is lower than that of the experiment. One possible explanation for the discrepancy in the high-temperature side of the PDFs in Fig. 6 is that the assumed equilibrium  $\text{OH}$  concentration of the co-flow in the DNS is lower than the real concentration in the experiment.

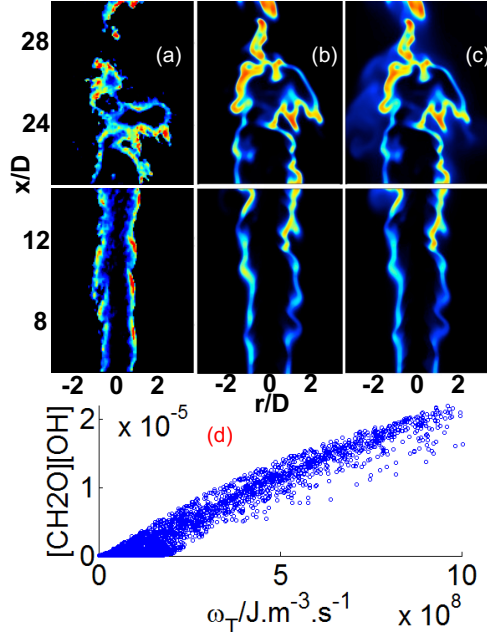


Figure 5. Instantaneous images of (a)  $[\text{CH}_2\text{O}][\text{OH}]$  from the experiment, (b)  $[\text{CH}_2\text{O}][\text{OH}]$  from the DNS, and (c) heat release rate from the DNS. (d) Scatter plots of  $[\text{CH}_2\text{O}][\text{OH}]$  versus heat release rate at  $x/D=24$  from the DNS.

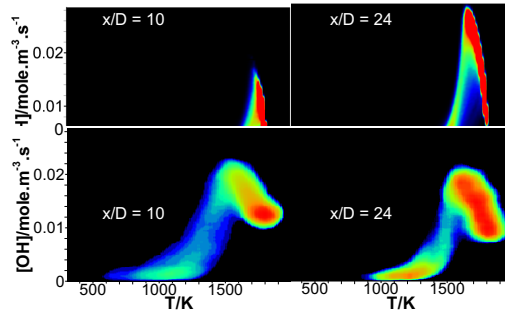


Figure 6. Comparison of joint PDFs of OH concentration and temperature of the (top) DNS and (bottom) measurements at  $x/D=10$  and

24.

## 5. Conclusions

DNS of a laboratory-scale turbulent premixed flame methane-air round jet was performed. The flame features high  $Ka$  and moderate  $Re$ . The DNS was validated against the experiment comprehensively for various quantities related to the turbulent burning velocity. First, the FSD based on OH image was compared between the DNS and experiment, and good agreement was obtained. The 2D and 3D flame surface densities were then compared for the DNS. The ratio  $\Sigma_3/\Sigma_2$  at the location of peak FSD is 1.14 and 1.35 at  $x/D=10$  and 24, respectively, which is comparable with other values reported for experimental flames.

Flame curvatures were also compared at various locations. The DNS results were almost identical to the experimental ones, indicating that the DNS and experiment have very similar wrinkling characteristics. The 2D and 3D flame curvatures evaluated on the progress variable iso-line/iso-surface were compared for the DNS. The 2D curvature PDFs were symmetric and their means were found to be near zero. The 3D flame curvature PDFs show, however, that the curvature distribution is positively skewed with a negative mean. The difference in behaviours between 2D and 3D was explained by analysing the flame geometry.

The product of OH and CH<sub>2</sub>O concentrations was found to provide a good surrogate of heat release rate in the present flame, implying that experimental results using this surrogate could be used to evaluate the stretch factor, and thus the local turbulent burning velocity according to the relationship expression  $S_T = S_L \cdot I_\theta \cdot \int \Sigma d\eta$ . In summary, the overall good agreement demonstrates the validity of the DNS with the reduced methane-air mechanism. In the future work, this DNS database will be used to explore various important features of high Ka flames and to assess models.

#### **Acknowledgement**

This work was supported by the Australian Research Council. This research used resources provided by the Pawsey Supercomputing Centre with funding from the Australian Government and the Government of Western Australia. The research was also supported by computational resources at Pawsey awarded through the National Computational Merit Allocation Scheme. The work at Sandia National Laboratories was supported by the Division of Chemical Sciences, Geosciences and Biosciences, the Office of Basic Energy Sciences, the US Department of Energy (DOE). Sandia National Laboratories is a multiprogram laboratory operated by Sandia Corporation, a Lockheed Martin Company, for the US Department of Energy under contract De-AC04-94-AL85000. The work at Lund University was supported by the Swedish Energy Agency and the ERC Advanced Grant, TUCLA.

## Reference

- (1) T. Lieuwen, V. McDonnell, E. Petersen, D. Santavicca, *J. Eng. Gas Turbines Power* 130 (2008) 011506.
- (2) N. Peters, *Turbulent Combustion*, Cambridge University Press, Cambridge, UK, 2000.
- (3) C. Meneveau, T. Poinso, *Combust. Flame* 86 (1991) 311-332.
- (4) J.H. Chen, H.G. Im, *Proc. Combust. Inst.* 27 (1998) 819-826.
- (5) E.R. Hawkes, J.H. Chen, *Combust. Flame* 138 (2004) 242-258.
- (6) E.R. Hawkes, J.H. Chen, *Proc. Combust. Inst.* 30 (2005) 647-655.
- (7) N. Chakraborty, S. Cant, *Combust. Flame* 137 (2004) 129-147.
- (8) M. Tanahashi, Y. Nada, Y. Ito, T. Miyauchi, *Proc. Combust. Inst.* 29 (2002) 2041-2049.
- (9) A.J. Aspden, M.S. Day, J.B. Bell., *J. Fluid mech.* 680 (2011) 287-320.
- (10) H. Carlsson, R. Yu, X. Bai, *Proc. Combust. Inst.* 35 (2015) 1425-1432.
- (11) B. Savard, B. Bobbitt, G. Blanquart, *Proc. Combust. Inst.* 35 (2015) 1377-1384.
- (12) R. Sankaran, E. R. Hawkes, J. H. Chen, et al., *Proc. Combust. Inst.* 31 (2007) 1291-1298.
- (13) R. Sankaran, E. R. Hawkes, C. S. Yoo, J. H. Chen, et al., *Combust. Flame* 162 (2015) 3294-3306.
- (14) E. R. Hawkes, O. Chatakonda, H. Kolla, A.R. Kerstein, J.H. Chen, *Combust. Flame* 159 (2012) 2690-2703.
- (15) O. Chatakonda, E.R. Hawkes, A.J. Aspden, A.R. Kerstein, H. Kolla, J.H. Chen, *Combust. Flame* 160 (2013) 2422-2433.
- (16) J.B. Bell, M.S. Day, I.G. Shepherd, M. R. Johnson, R. K. Cheng, J. F. Grcar, V. E. Beckner, M. J. Lijewski, *Proc. Natl. Acad. Sci. USA* 102 (2005) 10006-10011.
- (17) J. B. Bell, M. S. Day, J. F. Grcar, M. J. Lijewski, J. F. Driscoll, S. A. Filatyev, *Proc. Combust. Inst.* 31 (2007) 1299-1307.
- (18) M. Day, S. Tachibana, J. Bell, M. Lijewski, V. Beckner, R. K. Cheng, *Combust. Flame* 162 (2015) 2148-2165.
- (19) M. S. Mansour, N. Peters, Y.-C. Chen, *Proc. Combust. Inst.* 27 (1998) 767-773.

- (20) M. J. Dunn, A. R. Masri, R. W. Bilger, *Combust. Flame* 151 (2007) 46–60.
- (21) B. Zhou, C. Brackmann, Q. Li, Z. Wang, P. Petersson, Z. Li, M. Aldén, X.-S. Bai, *Combust. Flame* 162 (2015) 2937–2953.
- (22) J.F. Driscoll, *Prog. Energy Combust. Sci.* 34 (2008) 91–134.
- (23) P.H. Paul, N.H. Najm, *Proc. Combust. Inst.* 27 (1998) 43–50.
- (24) B.O. Ayoola, R. Balachandran, J.H. Frank, E. Mastorakos, C.F. Kaminski, *Combust. Flame* 144 (2006) 1–16.
- (25) H. Yamaguchi, *Engineering Fluid Mechanics*, Springer Science & Business Media, 2008.
- (26) T. Passot, A. Pouquet, *J. Fluid Mech.* 118 (1987) 441–466.
- (27) S.B. Pope, *Turbulent Flows*, Cambridge University Press, Cambridge, UK, 2000.
- (28) J.H. Chen, A. Choudhary, B. de Supinski, et al., *Comput. Sci. Discovery* 2 (2009) 015001.
- (29) C.A. Kennedy, M.H. Carpenter, *Appl. Numer. Math.* 14 (4) (1994) 367–458.
- (30) C.A. Kennedy, M.H. Carpenter, R.M. Lewis, *Appl. Numer. Math.* 35 (3) (2000) 177–264.
- (31) T.F. Lu, C.K. Law, *Combust. Flame, Proc. Combust. Inst.* 154(4) 761-774, 2008.
- (32) P. Anselmo-Filho, S. Hochgreb, R.S. Barlow, R.S. Cant, 32 (2009) 1763–1770.
- (33) E.R. Hawkes, R. Sankaran, J.H. Chen, *Proc. Combust. Inst.* 33 (2011) 1447–1454.
- (34) D. Veynante, G. Lodato, P. Domingo, L. Vervisch, E.R. Hawkes, *Exp. Fluids* 49 (2010) 267–278.
- (35) Y.C. Chen, R.W. Bilger, *Combust. Flame* 131 (2002) 400–435.
- (36) B.M. Deschamps, G.J. Smallwood, J. Prieur, D. R. Snelling, Ö. L. Gülder, *Proc. Combust. Inst.* 26 (1996) 427–435.

**Figure Captions:**

Figure 1. (a) Photograph of the turbulent flame from the experiment. (b) Schematic of the computational domain for DNS.

Figure 2. Comparison of the flame surface density  $\Sigma$  distribution: (a) DNS and (b) experiment. (c) Comparison of the integral of flame surface density in the radial direction  $\int \Sigma(x, r) dr$ .

Figure 3. Comparison of  $\Sigma$  along the radial direction at (a)  $x/D=10$  and (b)  $x/D=24$ .

Figure 4. Comparison of flame curvature PDFs at (a)  $x/D=10$  and (b)  $x/D=24$ .

Figure 5. Instantaneous images of (a)  $[\text{CH}_2\text{O}][\text{OH}]$  from the experiment, (b)  $[\text{CH}_2\text{O}][\text{OH}]$  from the DNS, and (c) heat release rate from the DNS. (d) Scatter plots of  $[\text{CH}_2\text{O}][\text{OH}]$  versus heat release rate at  $x/D=24$  from the DNS.

Figure 6. Comparison of joint PDFs of OH concentration and temperature of the (top) DNS and (bottom) measurements at  $x/D=10$  and 24.